Nonlinear Static Aeroelasticity of High Aspect Ratio Wing Aircraft by FEM and Multibody Methods

Michele Castellani[1], Jonathan E. Cooper[2] and Yves Lemmens[3]

Two procedures for the nonlinear static aeroelastic analysis of high aspect ratio wing aircraft subject to geometric nonlinearities are developed. The two approaches are based on the nonlinear Finite Element Method and on multibody dynamics and employ a linear aerodynamic formulation, respectively Doublet Lattice Method and strip theory. Static aeroelastic results in terms of wing integrated loads at various trim conditions for a very flexible aircraft testcase are presented and compared to the linear ones. Significant differences are found between a linear and a nonlinear approach and attention is drawn to the importance of the follower force effects of the aerodynamics and of considering large displacements and rotations, identified as the main sources of the discrepancies, for the static flight loads computation and subsequent structural sizing of the wing.

Nomenclature

$C_{L,\alpha}$ = lift curve slope
$\boldsymbol{D}$ = damping matrix of multibody beam element
D_{ijkl} = elastic stiffness fourth-order tensor
E_{ij} = Green-Lagrange strain tensor
e_0, e_1, e_2, e_3 = Euler parameters
EA, EI_y, EI_z, GJ =beam cross-sectional properties
$\boldsymbol{F_{aero}}$ = vector of aerodynamic forces and moments
$\boldsymbol{F_{el}}$ = vector of forces and moments of multibody beam element
$F_{Z,A/C}$ = total aircraft vertical aerodynamic force in global reference frame
f_i = i-th component of the applied force in nonlinear static analysis
g = gravitational constant
$\boldsymbol{K}$ = stiffness matrix of multibody beam element
$\boldsymbol{K_G}$ = FEM geometric stiffness matrix
$\boldsymbol{K_L}$ = FEM linear stiffness matrix
$\boldsymbol{K_{NL}}$ = FEM total nonlinear (tangent) stiffness matrix
K_I = controller integral gain
K_P = controller proportional gain
l = length of multibody beam element
$\boldsymbol{M}$ = mass matrix of multibody model
M_Y^{CG} = total pitching moment about aircraft center of gravity
m = aircraft mass
n_A = number of FEM structural degrees of freedom
n_z = vertical load factor
$\boldsymbol{Q_{AA}}$ = matrix of nodal aerodynamic forces due to nodal displacements and rotations
$\boldsymbol{Q_{AX}}$ = vector of nodal aerodynamic forces due to aircraft states
$\boldsymbol{q}$ = multibody generalized coordinates
q_∞ = dynamic pressure

[1] Marie Curie Early Stage Researcher – PhD Candidate, Department of Aerospace Engineering, University of Bristol, Bristol, UK, AIAA Student Member.
[2] Royal Academy of Engineering Airbus Sir George White Professor of Aerospace Engineering, Department of Aerospace Engineering, University of Bristol, Bristol, UK, AIAA Associate Fellow.
[3] Senior RTD Project Leader, Aerospace Centre of Competence, Siemens PLM Belgium, Leuven, Belgium.

$\boldsymbol{R}$ = rotation matrix
$\boldsymbol{r}$ = residual of nonlinear static analysis
$\boldsymbol{RB_{long}}$ = vector of longitudinal rigid body modes
S = area of aerodynamic strip
S_{ij} = second Piola-Kirchhoff stress tensor
t = time
$\boldsymbol{u_A}$ = vector of nodal displacements and rotations
$\boldsymbol{u_X}$ = vector of aircraft states
u_i = i-th component of the displacement field
u_j = j-th component of the displacement field
V = volume of structure
V_∞ = airspeed
α = angle of attack
β = angle of sideslip
$\Delta\boldsymbol{u}$ = vector of incremental displacements
$\delta(\cdot)$ = virtual variation operator
$\boldsymbol{\lambda}$ = Lagrange multipliers
λ = load step multiplier
ξ = multibody beam element damping factor
θ_l = l-th component of FEM nodal rotation

Superscripts

t = load increment of nonlinear static analysis
k = index of structural node

I. Introduction

THE European vision for aviation, Flightpath 2050[1], sets forth ambitious goals for the air transport system to meet by 2050. These include, among others, technological development and operational procedures to reduce aircraft CO_2 emissions, noise and NO_X emissions. Many research initiatives are currently adressed to investigate and develop design solutions leading to a more efficient and environmentally-friendly aircraft. The improvement of aerodynamic performance is at the forefront of these efforts and one of the most promising solution being sought is the design of high aspect ratio wings.

High aspect ratio wings can lead to significant fuel savings due to reduction in induced drag. Throughout the years, there has been a clear trend in large commercial transport aircraft towards wings with increasing aspect ratio, as proved by Figure 1, which reports the aspect ratio of wide-body airliners vs. the year of entry into service. For future designs, a number of high aspect ratio wing configurations are being considered and both Airbus[2] and Boeing[3] have published their own concept.

High aspect ratio wings nevertheless suffer from certain structural drawbacks. Due to the large span, the bending moment increases, resulting in higher structural weight. The drive toward Natural Laminar Flow wings has also renewed the interest in higher aspect ratio low swept wings. In such designs the beneficial gust alleviation due to bending-torsion coupling inherent in sweptback designs is absent[4]. In order to achieve an effective performance benefit, a lightweight wing design is though needed. This in turn leads to very flexible structures, where structural nonlinearities due to large displacements cannot be anymore neglected. The greater flexibility and lower structural frequencies could also result in a strong coupling between structural dynamics and rigid body (flight mechanics) modes and undesirable effects on the handling qualities.

The move away from linear behavior means that a non-conventional approach needs to be taken for the loads and aeroelastic analysis, in order to deal with geometric nonlinearites, and also the nonlinear aerodynamics and flight mechanics characteristics[5]. The ability to predict accurately limit loads, including these effects, already from the conceptual design phase is paramount in achieving an optimized structural sizing and eventually reaching success with these configurations.

A great deal of work has been done on the aeroelasticity of very flexible aircraft[6]. Most approaches have used ad-hoc nonlinear beam models coupled to aerodynamic models ranging from strip theory to unsteady vortex lattice method and CFD[7-13]. Less focus has instead been devoted to the use of multibody simulation for the modelling of high aspect ratio wings[14,15].

In this paper two structural modelling approaches, based on the Finite Element Method (FEM) and on multibody dynamics, are presented and compared to investigate the structural and static aeroelastic behavior of high aspect ratio wings which can show geometric nonlinearities due to large displacements and rotations. The study is limited to structures undergoing large displacements, but small strains, so that the material constitutive law is still linear, and to attached subsonic flow, so that a linear aerodynamic model can be employed.

The objective of the work is to develop a nonlinear aeroelastic trim procedure, where the nonlinearities are limited to the structure, in order to calculate flight loads for structural sizing in accordance with the static loads requirements prescribed by the certification specifications (EASA CS-25 and FAR-25). Static loads constitute an important set of the load cases to be considered to design the airframe and show compliance with the airworthiness regulations. Typically these conditions are critical for the inboard and mid wing and for certain parts of the fuselage of a large transport aircraft[16].Little work has been done on the impact of structural nonlinearities on flight loads; most of the efforts have instead been focused on the prediction of aeroelastic and flight dynamics instabilities. There is therefore a need in the industry to develop tools and methodologies able to take into account these effects and assess their importance in the design of future high aspect ratio wing aircraft.

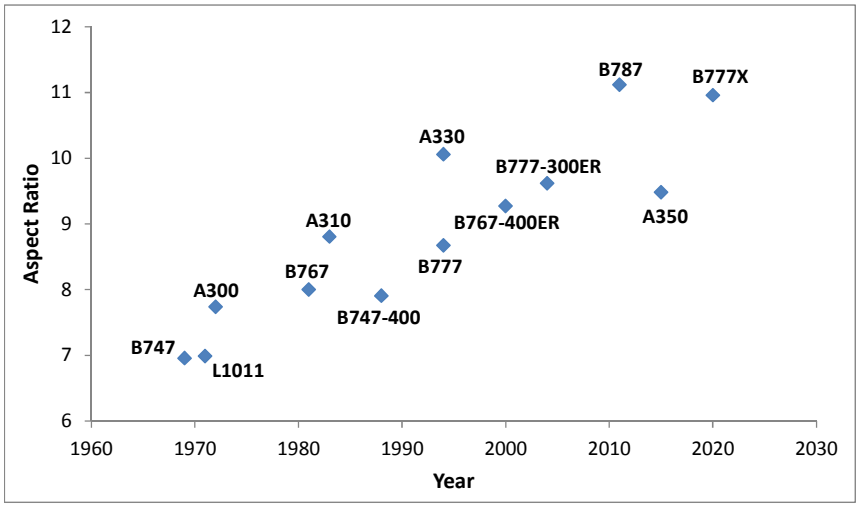

Figure 1. Aspect ratio of wide-body airliners vs. year of entry into service.

II. Modelling of High Aspect Ratio Wings

In the following section, the two methodologies applied for the modelling of high aspect ratio wings are described, introducing both the structural and aerodynamic models adopted.

The test case selected for the present work is a very flexible High Altitude Long Endurance Unmanned Aerial Vehicle (HALE UAV), first presented by Hodges et al.[7], which features a rectangular unswept wing with an aspect ratio of 32. Table 1 summarizes the main geometric properties of the aircraft and it is deemed a good test case being tailored to highlight extreme structural nonlinearities and thus challenge the capabilities of the proposed methods.

Table 1. Main properties of the HALE UAV test case.

Property	Value
Mass	74.4kg
Wingspan	32m
Chord	1m
AR	32
Wing Centre of Gravity	50% chord
Wing Elastic Axis	50% chord
Wing Aerodynamic Centre	25% chord

A. Nonlinear Finite Element Method

The first approach presented is based on the nonlinear Finite Element Method. FEM is nowadays a reliable and powerful tool for nonlinear structural analysis in various fields of engineering and science. It is largely used during an aircraft development and certification cycle and models of variable fidelity, ranging from simple stick to full 3D Global FEM (GFEM), are available throughout the various stages of the design process. Therefore, for the purpose of developing methodologies to predict aeroelastic response and flight loads with structural nonlinearities, there is a clear advantage in employing a tool which is already a standard in the aviation industry practice, since this would also ease the model generation phase or even lead to the sharing/adaptation of the same models between different disciplines (stress, loads and aeroelasticity etc.).

The FEM code chosen for this work is NX Nastran[17], which provides the capability to model the structure with 1D, 2D and 3D elements and can take into account geometric and material nonlinearities.

The structural nonlinearities considered in the present work arise from large displacements and rotations and from follower force effects, i.e. geometric nonlinearities; the strains are still assumed small and the material constitutive law linear. A brief introduction on static nonlinear structural analysis is outlined hereafter; the theoretical background follows Bathe[18].

When a structure undergoes large displacements, the governing equilibrium equations must be established on the current deformed geometry and the strain-displacement relationship must include second order terms. Geometric nonlinear problems are dealt with in an incremental and iterative fashion, that is the solution is sought partitioning the external loads into load steps applied incrementally once the previous converged configuration has been reached, after sub-iterating at each load step through a Newton-Raphson technique. The process is depicted by Figure 2.

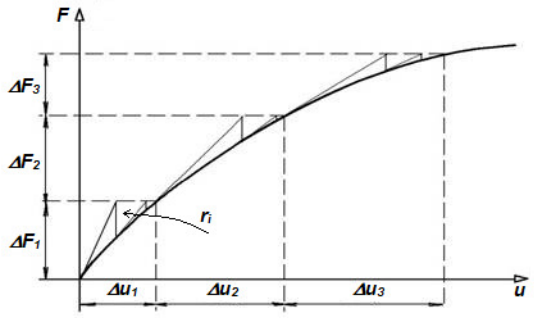

Figure 2. Solution process for nonlinear static analysis.

Two approaches have been proposed to this purpose: Total Lagrangian Formulation (TLF) and Updated Lagrangian Formulation (ULF). The latter is used by Nastran and briefly presented in the following.

In the ULF, the equations and the variables are formulated in the current (at time/increment t) deformed configuration and the strain-displacement relationship is expressed by the Green-Lagrange finite strain tensor

$$E_{ij}^{t} = \frac{1}{2}\left[\frac{\partial u_i^t}{\partial x_j} + \frac{\partial u_j^t}{\partial x_i} + \frac{\partial u_k^t}{\partial x_i}\frac{\partial u_k^t}{\partial x_j}\right] \tag{1}$$

which includes second order terms. The conjugate second Piola-Kirchhoff stress tensor is given by the linear constitutive equation

$$S_{ij}^{t} = D_{ijkl}E_{kl}^{t} \tag{2}$$

D_{ijkl} being the elastic stiffness tensor under the assumption of a linear constitutive law. The strains can be decomposed into a linear and a nonlinear part

$$E_{ij}^{t} = e_{ij}^{t} + \eta_{ij}^{t} \tag{3}$$

and the stresses respectively in the stresses at equilibrium and those at the incremental step

$$S_{ij}^{t+\Delta t} = S_{ij}^{t} + \tau_{ij} \tag{4}$$

The static equilibrium equation, obtained from the principle of virtual displacements, reads

$$\int_{V^t} S_{ij}^{t+\Delta t} \delta E_{ij}^{t+\Delta t} dV^t = f_i^{t+\Delta t} \delta u_i^t \tag{5}$$

where $f_i^{t+\Delta t}$ are the external loads. Substituting the stress and strain tensors in the previous equation and linearizing it, in the framework of a FE discretization of the structure, leads to

$$[\boldsymbol{K_L^t} + \boldsymbol{K_G^t}]\boldsymbol{\Delta u} = \boldsymbol{r^t} \tag{6}$$

At each load increment, the equation is solved iteratively by a (modified) Newton-Raphson procedure (see Figure 2). The RHS represents the residual (difference between applied and internal loads at the current step t) whereas $\boldsymbol{K_L^t}$ and $\boldsymbol{K_G^t}$ are the linear and nonlinear (or geometric) stiffness matrices, assembled in the current displaced configuration; the sum of the two is the tangent stiffness matrix. $\boldsymbol{K_G^t}$ stems from the quadratic terms of the Green-Lagrange tensor and takes into account the effects of the pre-stress.

To test the proposed modelling methodology, a stick model of the very flexible HALE UAV has been generated based on the data available in Hodges[7]. The stick-beam representation has been the common choice for high aspect ratio wings in many previous publications[7-13], being well apt to accurately model these slender structures, whose behavior is dominated by the vertical bending, with a reduced computational time compared to a 3D GFEM of the wing box.

The structural model comprises 32 beam elements (CBEAM) along the semi-span of the wing, lumped masses attached to each structural node and a single lumped mass representing the fuselage and payload. The horizontal tailplane is represented too by beam elements.

The aerodynamic model of the lifting surfaces employs the Doublet Lattice Method[19] (DLM), which, in the steady case considered, reduces to Hedman's vortex lattice[20]. The Infinite Plate Spline is used to transfer forces and displacements between the structural and aerodynamic mesh. The complete model is shown in Figure 3.

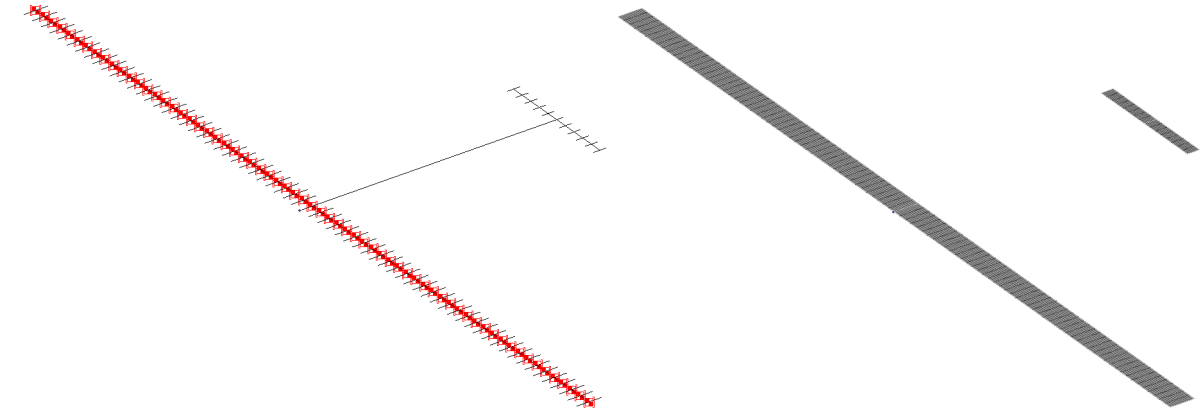

a) **b)**

Figure 3. Structural (a) and aerodynamic (b) mesh of the HALE UAV.

B. Multibody Dynamics

The second approach is based on multibody dynamics. Multibody dynamics simulation[21] is a convenient tool capable of simulating multiphysics systems with arbitrary types of nonlinearities and both rigid and flexible components. In the fixed-wing aeroelasticity field, it has been employed for the trim and simulation of maneuvering flexible aircraft coupled with aerodynamic methods of various levels of fidelity[22,23].

For the nonlinear aeroelasticity of very flexible aircraft, there have been applications of multibody simulation by Krüger et al.[14] and Zhao et al.[15], respectively for the study of the flight mechanics stability of a HALE configuration and for the aeroelastic stability analysis and flight control in maneuvers of a UAV-like flexible aircraft.

Multibody dynamics allows for arbitrary large displacements and rotations, generic force definition (follower and non-follower) and inherent coupling between large rigid body motion, linked to flight mechanics, and elastic deformation, without the need of developing dedicated formulations. These are distinct advantages that make multibody dynamics attractive for the analysis of high aspect ratio wings including structurally nonlinear effects.

The multibody software employed for this work is LMS Virtual.Lab Motion v.13.1[24].

In the following the equations of motion of a multibody system are briefly outlined (for more details see Shabana[21]). Each body is described by a set of Cartesian coordinates, identifying the location of its center of gravity in the global reference frame. The vector of the generalized coordinates of the $i-th$ body is thus

$$\boldsymbol{q}_i = \{x \;\; y \;\; z \;\; e_0 \;\; e_1 \;\; e_2 \;\; e_3\}^T \tag{7}$$

where x, y, z are the Cartesian coordinates and e_0, e_1, e_2, e_3 the (redundant) Euler parameters used to describe the orientation of the body and to avoid the singularity occurring with other representation, e.g. Euler angles.

The bodies in the system are connected together by joints and kinematic relationships, which are expressed as general nonlinear algebraic constraint equations

$$C(\boldsymbol{q}, \dot{\boldsymbol{q}}, t) = 0 \tag{8}$$

Differentiating twice these equations with respect to time t, one obtains the kinematic acceleration equations

$$\boldsymbol{C_q}\ddot{\boldsymbol{q}} = \boldsymbol{Q_d} \tag{9}$$

where $\boldsymbol{Q_d} = -\boldsymbol{C}_{tt} - \left(\boldsymbol{C_q}\dot{\boldsymbol{q}}\right)_{\boldsymbol{q}}\dot{\boldsymbol{q}} - 2\boldsymbol{C}_{\boldsymbol{qt}}\dot{\boldsymbol{q}}$. The dynamic equations of motion, e.g. derived from Lagrange method, are, for the $i-th$ body,

$$\boldsymbol{M}_i\ddot{\boldsymbol{q}}_i + \boldsymbol{C}_{\boldsymbol{q},i}^T\boldsymbol{\lambda}_i = \boldsymbol{Q}_{\boldsymbol{e},i} + \boldsymbol{Q}_{\boldsymbol{v},i} \tag{10}$$

with $\boldsymbol{M}_i$ mass matrix, $\boldsymbol{\lambda}_i$ vector of Lagrange multipliers, $\boldsymbol{Q}_{\boldsymbol{e},i}$ vector of generalized applied forces and $\boldsymbol{Q}_{\boldsymbol{v},i}$ vector of velocity dependent terms. Adding the kinematic relationships to the equations of motion, a system of nonlinear Differential Algebraic Equations (DAE) describing the kinematics and dynamics of a multibody system is obtained

$$\begin{bmatrix} \boldsymbol{M} & \boldsymbol{C}_{\boldsymbol{q}}^T \\ \boldsymbol{C_q} & \boldsymbol{0} \end{bmatrix} \begin{Bmatrix} \ddot{\boldsymbol{q}} \\ \boldsymbol{\lambda} \end{Bmatrix} = \begin{Bmatrix} \boldsymbol{Q_e} + \boldsymbol{Q_v} \\ \boldsymbol{Q_d} \end{Bmatrix} \tag{11}$$

The equations are nonlinear, being the matrices function of the vector of generalized coordinates itself, and are solved by a Backward Differentiation Formula integrator.

The bodies can be considered either as rigid or flexible. The most common approach to model flexibility is a modal representation based on Component Mode Synthesis from FEM[25], which adds to the generalized coordinates the modal participation factors of each mode used to represent a body's flexibility. This however limits the applicability to linear structures with small elastic displacements. Formulations based on nonlinear FE beams[26] and generic nonlinear FEM elements[27] have been also proposed to this purpose.

The work presented in this paper employs a simpler yet efficient approach to model a flexible wing with arbitrary large elastic displacements. It is based on the discretization of the wing by a series of rigid bodies, to which inertial properties are assigned, interconnected by beam force elements, representing the stiffness distribution. In literature this modelling technique has been known as the Finite Segment approach[28] and it has been successfully used for very flexible aircraft[14,15]. Since the multibody formulation allows arbitrarily large rigid body motion, each wing section can undergo large displacements and rotations and the ensuing internal forces are determined based on this displacement field. Each multibody beam element connects two consecutive rigid bodies and has a stiffness matrix derived from FE linear 6 Degrees Of Freedom (DOFs) beam theory and the usual cross-sectional properties

(EA, EI, GJ) are assigned to it. The relative forces and moments $\boldsymbol{F_{el}}$ exchanged between two connected bodies are calculated as

$$\boldsymbol{F_{el}} = \boldsymbol{K}\boldsymbol{x} + \boldsymbol{D}\dot{\boldsymbol{x}} \tag{12}$$

where $\boldsymbol{x}$ and $\dot{\boldsymbol{x}}$ are the relative displacements and velocities $\boldsymbol{K}$ and $\boldsymbol{D}$ are the linear stiffness and damping matrices. The stiffness matrix is a 6x6 symmetric matrix given by

$$\boldsymbol{K} = \begin{bmatrix} \frac{EA}{l} & 0 & 0 & 0 & 0 & 0 \\ 0 & \frac{12EI_z}{l^3} & 0 & 0 & 0 & \frac{-6EI_z}{l^2} \\ 0 & 0 & \frac{12EI_y}{l^3} & 0 & \frac{6EI_y}{l^2} & 0 \\ 0 & 0 & 0 & \frac{GJ}{l} & 0 & 0 \\ 0 & 0 & \frac{-6EI_z}{l^2} & 0 & \frac{4EI_y}{l} & 0 \\ 0 & \frac{6EI_y}{l^2} & 0 & 0 & 0 & \frac{4EI_z}{l} \end{bmatrix} \tag{13}$$

The damping is proportional to the diagonal of the stiffness matrix by a damping factor ξ, i.e. $\boldsymbol{D} = \xi \cdot diag(\boldsymbol{K})$.

Figure 4 reports the HALE UAV multibody model, with a zoom-up of the wing showing the discretization and interconnection of the rigid bodies. The fuselage and horizontal tailplane are introduced as a single rigid body at the total center of gravity, i.e. no flexibility effect on the horizontal tailplane is considered. The wing adopts the same discretization as the FE model, 32 rigid bodies along each semispan, however an important point to highlight is that in the multibody the DOFs are placed at the center of gravity of each rigid body, therefore are not co-located with the FEM ones, which are placed at the structural nodes.

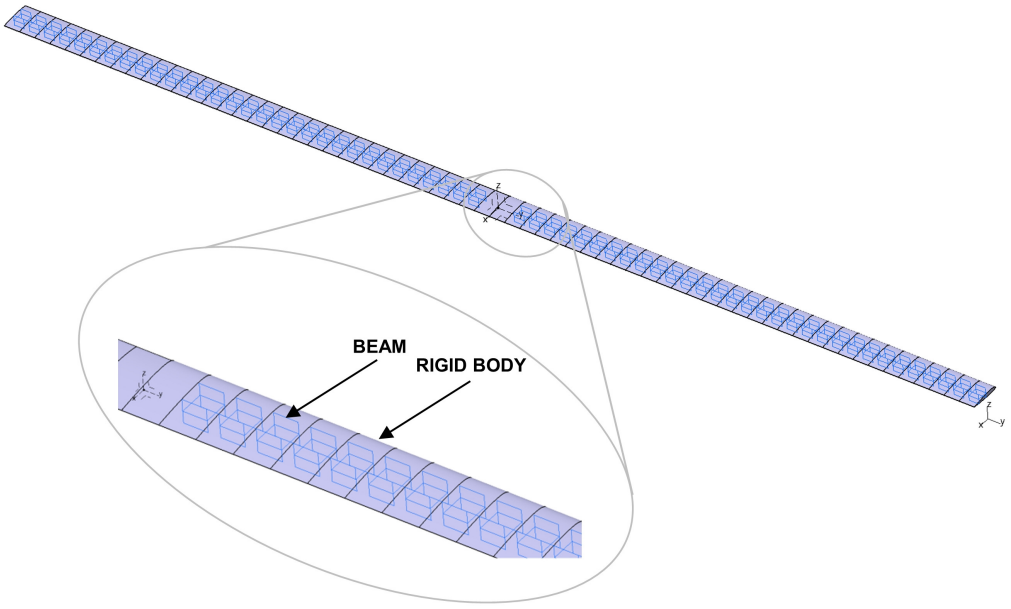

Figure 4. Multibody model of the HALE UAV.

The aerodynamic model is based on strip theory. Though more simplistic than higher-fidelity methods, this approach is suitable and still accurate for high aspect ratio wings. To further support this choice, strip theory can be straightforwardly integrated with the wing Finite Segment representation because no interpolation process is required between the aerodynamic and structural meshes: the aerodynamic forces and moments are applied at the aerodynamic center of each rigid body, which represents a strip.

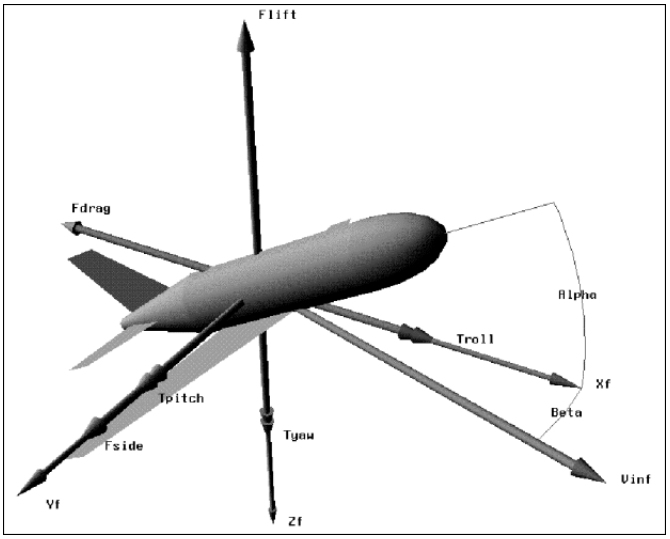

Figure 5. Aerodynamic reference frame, angles and forces definition for multibody strip theory (from[24]).

Referring to Figure 5, the reference frame $(X_{f,}Y_{f,}Z_{f,})$ is the stability axis system used in flight mechanics and the aerodynamic forces are given by

$$F_j = q_\infty S\left(C_{j0} + C_{j,\alpha}\alpha + C_{j,\beta}\beta + C_j(\alpha,\beta)\right) \tag{14}$$

where j represents drag C_D, lift C_L or sideforce C_S, and the aerodynamic moments by

$$T_j = q_\infty S\left(C_{j0} + C_{j,\alpha}\alpha + C_{j,\beta}\beta + C_j(\alpha,\beta)\right) \tag{15}$$

where j represents rolling $C_{\mathcal{L}}$, pitching C_M or yawing moment C_N. The aerodynamic coefficients can be a nonlinear function of the angle of attack and sideslip through the term $C_i(\alpha,\beta)$, for instance derived from airfoil experimental data, and stall effects can in this way be included.

Indicating with u, v and w the relative airflow velocities in body axes for each strip, the local angle of attack α and local angle of sideslip β are calculated as

$$\alpha = \sin^{-1}\frac{w}{V_\infty \cos\beta} \tag{16}$$

$$\beta = \sin^{-1}\frac{v}{V_\infty} \tag{17}$$

and include all the contribution due to the aircraft states (aircraft angle of attack, sideslip and angular rates) and to the elastic deformation of each section.

In order to have a similar aerodynamic representation to the FEM approach presented before, which uses linear DLM aerodynamics, an equivalent sectional $C_{L,\alpha}$ is computed from DLM, thus effectively correcting the strip theory for tip effects, and it is shown in Figure 6.

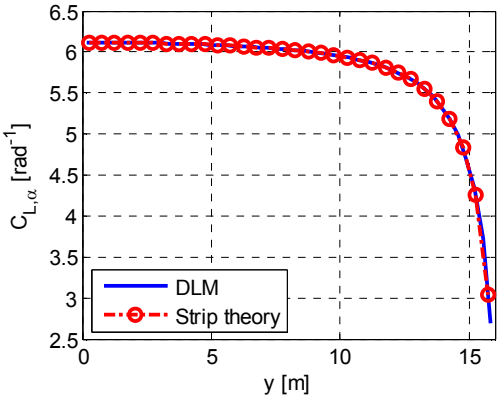

Figure 6. Span distribution of lift curve slope used in the strip theory vs. DLM reference value.

III. Nonlinear Aeroelastic Trim

The following section describes the nonlinear static aeroelastic trim procedures developed in the nonlinear FEM and multibody approach. To develop the methods, the trim is limited to the aircraft longitudinal plane.

A. Nonlinear Finite Element Method

A procedure for the nonlinear static aeroelastic trim of the free-flying aircraft based on the nonlinear static FE analysis available in NX Nastran (SOL106) has been developed and applied to high aspect ratio wings in order to compute flight loads. Aeroelastic tools commonly used in industrial applications lack the capability of performing aeroelastic trim analysis on nonlinear structures. In recent years, few approaches were proposed to develop such capabilities in a FE framework. Demasi et al.[29,30] presented two methodologies integrating linear unsteady aerodynamics with a nonlinear FE model of a joined wing configuration represented as a plate-like structure. Other efforts focused on the loose coupling of FEM/CFD codes[31] and on the coupling of Nastran and lifting-line theory[32].

The method presented in this work formulates the structurally nonlinear static aeroelastic trim in the FE framework as an integrated problem, adding to the structural equations the aircraft trim equations and the linear aerodynamics with an AIC (Aerodynamic Influence Coefficients) representation, similarly to a standard linear aeroelastic trim problem such as that solved by Nastran SOL144. The advantage of this procedure is that it makes full use of the vast and powerful modelling capabilities of nonlinear FEM, ranging from simple stick to fully 3D models, and, being an integrated approach, is efficient and does not resort on the coupling of separate structural and aerodynamic codes. Thus it reduces the effort both in terms of computation and analysis setup, which is the same as that of a standard linear trim. Besides, the applicability is not limited to a DLM aerodynamics, but, thanks to the integrated formulation and the AIC representation, higher-fidelity linear methods can be employed, such as 3D panel method as proposed recently by Kier[33], and also corrected for transonic effects from CFD or wind tunnel by weighting coefficients, as it is done in the standard industrial practice.

Starting from the equations of a purely nonlinear structural static problem Eq. (1), the aeroelastic trim analysis of a free-flying aircraft is tackled. The external loads comprise gravitational and aerodynamic forces, the latter being dependent on the states of the aircraft $\boldsymbol{u_X}$ (angle of attack, sideslip, angular rates, control surfaces deflections) and on the structural displacements $\boldsymbol{u_A}$. Since the aerodynamic model is linear, the forces can be expressed as

$$\boldsymbol{F_{aero}} = q_\infty(\boldsymbol{Q_{AA}u_A} + \boldsymbol{Q_{AX}u_X}) \tag{18}$$

where $\boldsymbol{Q_{AA}}$ and $\boldsymbol{Q_{AX}}$ are the matrices of the aerodynamic forces on the FE nodes due to the nodes' displacements and to the aircraft states.

Considering the longitudinal trim and assuming that the equilibrium in the longitudinal degree of freedom is always satisfied by thrust equalling the drag, the free-flying aircraft is trimmed at a specific vertical load factor n_z and with zero pitch acceleration $\dot{q}$ and pitch rate q, that is the two equilibrium equations

$$F_{Z,A/C} = n_z mg \tag{19}$$

$$M_Y^{CG} = 0 \tag{20}$$

must be satisfied. The total vertical aerodynamic force $F_{Z,A/C}$ and pitching moment about the Center of Gravity (CG) M_Y^{CG} are given by

$$\begin{Bmatrix} F_{Z,aero} \\ M_Y^{CG} \end{Bmatrix} = q_\infty \boldsymbol{RB}_{\boldsymbol{long}}^T (\boldsymbol{Q}_{\boldsymbol{AA}} \boldsymbol{u}_{\boldsymbol{A}} + \boldsymbol{Q}_{\boldsymbol{AX}} \boldsymbol{u}_{\boldsymbol{X}}) \tag{21}$$

where $\boldsymbol{RB}_{\boldsymbol{long}}$ is the matrix of the vertical translation and pitching rotation rigid body modes needed to compute the force and moment resultants about the CG from the distributed nodal aerodynamic forces. The rigid body matrix $\boldsymbol{RB}_{\boldsymbol{long}}$ is updated throughout the analysis based on the current shape, therefore both the structural and trim equations are written in the displaced configuration.

The matrix of the aerodynamic forces due to the structural displacement $\boldsymbol{Q}_{\boldsymbol{AA}}$ can be interpreted as an aerodynamic stiffness to be added to the structural stiffness and, augmenting the structural nonlinear static equations with the two longitudinal trim equations, the nonlinear aeroelastic trim problem can be formulated as

$$\begin{bmatrix} \boldsymbol{K}_{\boldsymbol{NL}} - \lambda(q_\infty \boldsymbol{Q}_{\boldsymbol{AA}}) & -\lambda(q_\infty \boldsymbol{Q}_{\boldsymbol{AX}}) \\ \lambda(q_\infty \boldsymbol{RB}_{\boldsymbol{long}}^T \boldsymbol{Q}_{\boldsymbol{AA}}) & \lambda(q_\infty \boldsymbol{RB}_{\boldsymbol{long}}^T \boldsymbol{Q}_{\boldsymbol{AX}}) \end{bmatrix}_i \begin{Bmatrix} \Delta \boldsymbol{u}_{\boldsymbol{A}} \\ \Delta \boldsymbol{u}_{\boldsymbol{X}} \end{Bmatrix}_i = \begin{Bmatrix} \boldsymbol{r}_{struct} \\ \boldsymbol{r}_{trim} \end{Bmatrix}_i \tag{22}$$

where the subscript i indicates the current load increment. The RHS term represents the residual of both the structural and trim equations, where the external loads applied are gravitational forces at the specified n_z and aircraft mass.

Like in the standard nonlinear structural analysis, the solution is carried out in incremental steps and sub-iterations: the gravitational and aerodynamic loads are scaled by a load multiplier λ that increases gradually from 0 to 1. At each load step the converged solution is found iteratively and then the next load step applied until the final value is reached. To improve convergence, the line search method is applied to the Newton-Raphson procedure and two convergence criteria are employed, one based on the work and one on the displacements[17]. Since to perform a static analysis the aircraft must be constrained in at least 6 DOFs in order to remove singularities from the stiffness matrix, a further check on convergence is done on the magnitude of the constraint forces, which must be close to zero for a free-flying aircraft in trimmed state.

In addition to the geometric nonlinearities due to large displacements, the other important source of nonlinearity neglected in a linear analysis is the follower force effect due to a change of orientation of the applied loads as the structure deforms. Aerodynamic forces fall indeed in this category and this effect must be taken into account in order to compute accurately the integrated loads along the wing.

This entails rotating the aerodynamic forces matrices $\boldsymbol{Q}_{\boldsymbol{AA}}$ and $\boldsymbol{Q}_{\boldsymbol{AX}}$, which are generated in the undeformed condition, at each iteration of the Newton-Raphson procedure based on the previous converged deformed configuration (represented by the subscript i). Specifically, $\boldsymbol{Q}_{\boldsymbol{AA}}$ is updated as

$$\boldsymbol{Q}_{\boldsymbol{AA},i+1} = \boldsymbol{R}_i \boldsymbol{Q}_{\boldsymbol{AA},i} \boldsymbol{R}_i^T \tag{23}$$

where $\boldsymbol{R}_i$ collects the rotation matrices $\boldsymbol{R}_i^k$ of each $k-th$ structural node where aerodynamic forces and moments are applied (multiplying both the 3 forces and the 3 moments), that is

$$\boldsymbol{R}_i^k = \begin{bmatrix} c_y c_z & s_x s_y c_z - c_x s_z & c_x s_y c_z + s_x s_z \\ c_y s_z & s_x s_y c_z + c_x c_z & c_x s_y s_z - s_x c_z \\ -s_y & s_x c_y & c_x c_y \end{bmatrix} \tag{24}$$

with $c_l = \cos\theta_l$ and $s_l = \sin\theta_l$ for $l = x, y, z$ and θ_l are the three rotations of the node in the global FE reference frame. The LHS multiplication rotates the aerodynamic force, in the DLM assumption normal to each aerodynamic panel, to the panel new orientation whereas the RHS multiplication updates the normalwash boundary conditions by rotating the panel's normal vector.

For the longitudinal trim case, the aerodynamic matrix due to the aircraft states has two columns corresponding to the aircraft angle of attack and elevator deflection, i.e. $\boldsymbol{Q}_{\boldsymbol{AX}} = [\boldsymbol{Q}_{\boldsymbol{A\alpha}} \ \boldsymbol{Q}_{\boldsymbol{A\delta}}]$. Considering that the displacements of

the horizontal tailplane are still within the assumption of small displacements and rotations, only the former is updated as

$$\boldsymbol{Q}_{A\alpha,i+1} = \boldsymbol{R}_i \boldsymbol{R}_{\alpha,i} \boldsymbol{Q}_{A\alpha,i} \tag{25}$$

where $\boldsymbol{R}_{\alpha,i}$ is a $n_A \times 1$ matrix which updates the local rigid angle of attack following the change of orientation of the aerodynamic panel's normal vector and is given by collecting the nodal rotation matrix $\boldsymbol{R}_{X,i}^{k}$ (multiplying both the 3 forces and the 3 moments) such that

$$\boldsymbol{R}_{\alpha,i} = \begin{bmatrix} c_x c_y & 0 & 0 \\ 0 & c_x c_y & 0 \\ 0 & 0 & c_x c_y \end{bmatrix} \tag{26}$$

The rotations of Eqs. (23) and (25) generate forces along the global FE X-axis, i.e. parallel to the airflow. In order to be consistent with the DLM assumption of aerodynamic force only normal to the panel, this longitudinal force component is zeroed out.

The procedure described above has been implemented within the nonlinear static solution of NX Nastran through a DMAP (Direct Matrix Abstract Programming) code[34], taking advantage of the highly optimized routines provided by Nastran for matrix manipulation and linear algebra.

B. Multibody Dynamics

In the multibody approach, the trim solution is sought by performing a dynamic settling simulation with the implementation of controllers in order to drive the aircraft to the steady trimmed state. Even though the trim is a static problem, in a multibody environment, which is intrinsically a dynamic simulation, it is more efficient to perform such analysis rather than a static solution, which would on the other hand require a modification of the solver to add constraint equations for the velocities[35]. The disadvantage of this procedure is that the gains must be adapted to the flight conditions and mass configurations (gain scheduling).

Considering the longitudinal trim, three control objectives are identified: the target vertical load factor n_z, zero pitch acceleration and the target flight speed V_∞. The trim is accomplished by driving the aircraft, which is constrained on the the longitudinal plane by a planar joint, through two control inputs, the elevator control force and the thrust, the former both to drive the aircraft at the trim angle of attack and to achieve the pitching moment equilibrium about the CG and the latter to set the aircraft at the desired flight speed.

The block diagrams of the two controllers are shown in Figure 7. For the vertical and rotational degrees of freedom, the vertical CG velocity $\dot{z}_{CG}$ and the pitch rate about the CG $\dot{\theta}_{CG}$ are measured in the aircraft body reference frame and must be driven to zero. In this way, at the trimmed condition, the total vertical acceleration $\ddot{z}_{CG}$ and the pitching acceleration $\ddot{\theta}_{CG}$ are both zero, i.e. the lift equals the weight times the load factor and the total pitching moment about the CG is zero. The controller is an integral-only type and the total control output, the elevator force, is the sum of the contributions of the vertical velocity and pitch rate integral terms. Butterworth 2nd order low-pass filters are used to remove high-frequency oscillations of the measured variables. Once a steady state is reached, the error is set to zero in order to disable the trim controller, for subsequent gust and maneuver analyses, but keeping constant the elevator trim force acting on the aircraft thanks to the integral actions. Similarly, for the longitudinal degree of freedom, the aircraft forward speed is measured and driven to the target flight speed by a proportional-only controller. A low-pass filter and a steady state check are applied as well.

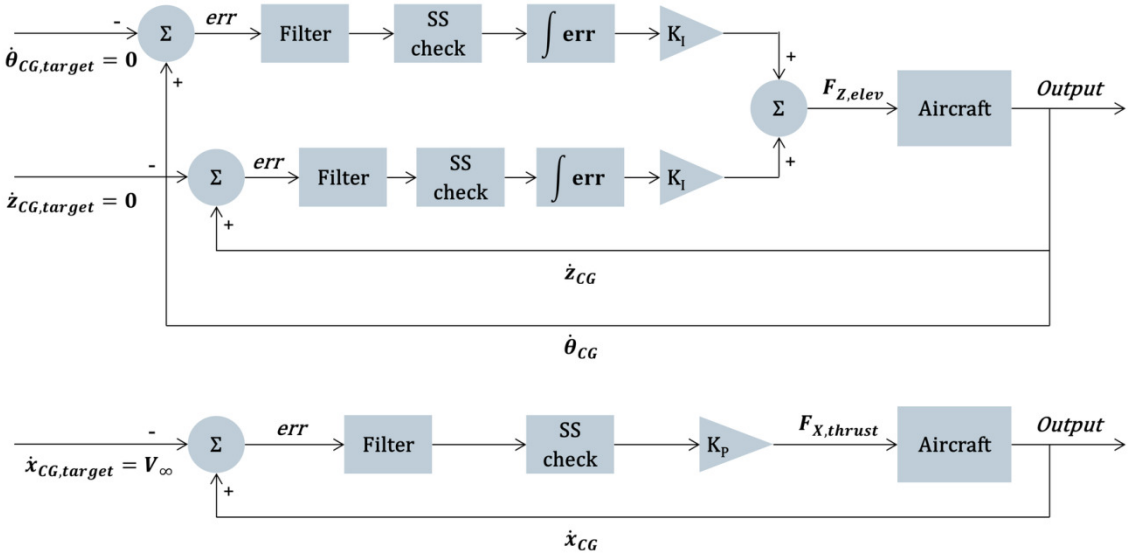

Figure 7. Schemes of the PID controllers implemented in the multibody simulation to trim the aircraft.

IV. Results

This section presents the results of the analyses performed on the HALE UAV test case comparing the FEM and multibody methods. First, the structural and mass modelling is validated by carrying out nonlinear static and pre-stressed normal modes analyses; nonlinear aeroelastic trim analyses at 1g varying the airspeed are then performed and the trim solution and wing integrated loads obtained with the two methods are compared.

A. Nonlinear static analysis

Nonlinear static analyses are carried out on the HALE UAV half wing, clamped at the root, applying tip vertical forces of increasing magnitude (25N, 100N, 200N) as both non-follower and follower. For the FEM approach, the nonlinear static solution available in NX Nastran (SOL106) has been used and the results of the linear static analyses (SOL101) have also been obtained for the sake of comparison. For the multibody, the same analyses have been performed through the static equilibrium solver available in Virtual.Lab Motion.

Table 2 and Table 3 report the tip vertical displacement and the tip shortening vs. force comparing the linear static, nonlinear static and multibody solutions for, respectively, the non-follower and follower force cases. It is clear how the vertical tip displacement increasingly differs from the linear value as the magnitude of the force increases; for a tip force of 200N the linear analysis overpredicts the displacement by more than +50%. The other major effect not captured by the linear analysis is the lateral shortening of the wing, which reaches 21% of the semispan for the 200N case. This lateral shortening cannot be predicted by a linear structural formulation since it is a higher order effect; however neglecting it may lead to an inaccurate load prediction because the integrated loads computation along the wing, for a nonlinear analysis, is carried out on the actual deformed shape.

Comparing the non-follower and follower force results, there is of course no difference in the linear case, whereas in the nonlinear one a follower vertical force, being always normal to the wing axis, maximizes the bending and leads to higher deflections. The wing deformed shapes for the 200N tip force, both non-follower and follower, are shown in Figure 8.

Finally it can be noted that there is an excellent agreement, in a comparable computational time, between the nonlinear FEM and the multibody for all the analyses considered, despite the fact that the beam force element of the multibody is still based on a linear stiffness formulation.

Table 2. Tip vertical displacement and shortening vs. force, non-follower force.

	Linear FEM			*Nonlinear FEM*			*MBD*		
	25N	**100N**	**200N**	**25N**	**100N**	**200N**	**25N**	**100N**	**200N**
Tip vertical disp. [m]	1.707	6.827	13.653	1.687	5.865	8.993	1.687	5.866	8.995
Tip shortening [m]	0.0	0.0	0.0	-0.107	-1.355	-3.449	-0.107	-1.355	-3.450

Table 3. Tip vertical displacement and shortening vs. force, follower force.

	Linear FEM			*Nonlinear FEM*			*MBD*		
	25N	**100N**	**200N**	**25N**	**100N**	**200N**	**25N**	**100N**	**200N**
Tip vertical disp. [m]	1.707	6.827	13.653	1.700	6.409	10.754	1.700	6.405	10.757
Tip shortening [m]	0.0	0.0	0.0	-0.109	-1.650	-5.622	-0.109	-1.647	-5.626

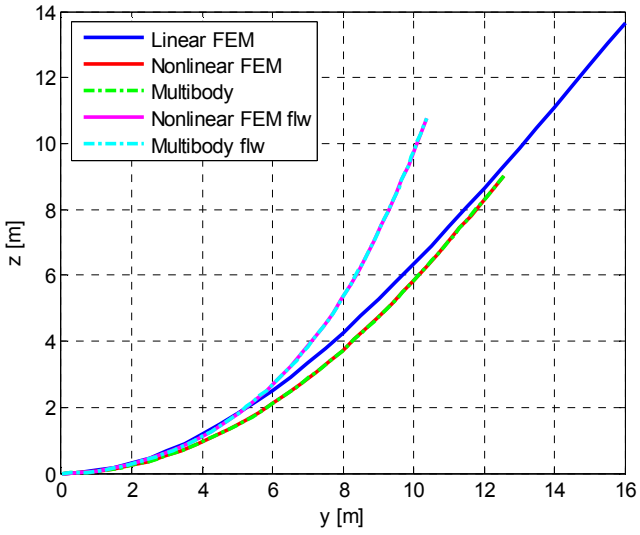

Figure 8. Wing deformed shape - tip force 200N.

B. Pre-stressed normal modes analysis

For very flexible aircraft, it is known that the deformation can have a substantial influence on the normal modes[36]. The pre-stressed natural frequencies and mode shapes of the clamped wing under a vertical (non-follower) static tip force are calculated at increasing force magnitude with the FEM and multibody. The former solves the classical eigenvalue problem with the tangent stiffness matrix output from a nonlinear static analysis. The latter instead performs a linearization about a static equilibrium by finite difference.

The first five natural frequencies vs. force are shown in Figure 9. The vertical bending frequencies (WB) are insensitive to the wing deformation and a good agreement between the two modelling techniques is achieved. The torsion (WT) and in-plane bending (WIB) modes, uncoupled in the undeformed configuration, show instead an increasing coupling with tip force magnitude and the associated frequencies a marked change. These findings agree with those reported by Hodges et al.[7]. For the lower frequency torsion/in-plane bending mode, the frequency predicted by the multibody is close to the FEM one, whereas for the higher frequency torsion/in-plane bending there is a greater difference.

The Modal Assurance Criterion between the FEM and multibody modes sets for a static tip force of 60N, Figure 10, confirms the discrepancies of the two torsion/in-plane bending modes (#2 and #5). The coupling predicted by the

multibody is less than the FEM prediction. This could be attributed to the different method used for the calculation of the modes and to the different beam formulation.

A sensitivity study on the number of rigid bodies along the wing of the multibody model has also been performed, in order to find an engineering trade-off between accuracy and computational burden.

Table 4 reports the percentage error on the natural frequencies at 60N static tip force, with respect to the FEM modal analysis, discretizing the wing with 16, 32 and 64 rigid bodies along the semispan. The error decreases increasing the number of bodies, as expected since the multibody beam formulation lacks the geometric stiffness matrix due to the pre-stress and the nonlinearities are indeed captured by the arbitrary large displacements of each rigid body. However, considering the computational time involved (shown in the last column of Table 4 and normalized to the time required by using 16 elements), which increases even further for a full dynamic simulation, it is deemed sufficient to model the wing with 32 bodies along the semispan.

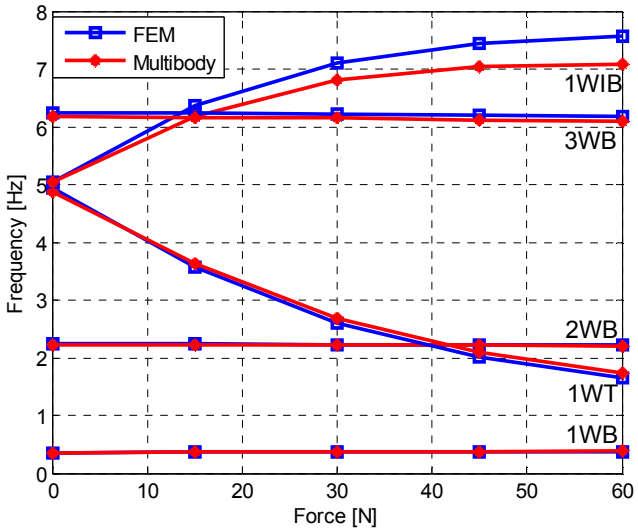

Figure 9. Natural frequencies vs. tip force - FEM vs. multibody.

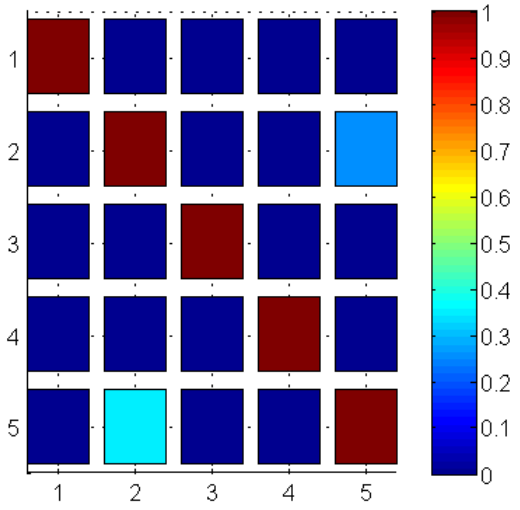

Figure 10. Modal Assurance Criterion applying 60N static tip force - FEM vs. multibody.

Table 4. Error of the multibody natural frequencies for 60N tip force (wrt FEM) varying the number of bodies.

# Bodies semispan	**1WB**	**2WB**	**1WT**	**1WIB**	**3WB**	**CPU time ratio [-]**
16	+4.1%	-1.2%	+14.4%	-15.9%	-2.5%	1
32	+1.9%	-0.3%	+5.2%	-6.3%	-1.2%	3.4
64	+0.8%	-0.5%	+2.5%	-5.1%	-0.7%	11.9

C. Nonlinear aeroelastic trim analysis

Nonlinear aeroelastic trim analyses on the HALE UAV have been performed with the FEM and multibody methods according to the procedures presented in Section III. For the sake of comparison, standard linear trim analyses have been performed as well by Nastran SOL144 (static aeroelastic solution).

The load factor is set at 1g, the density at 0.0889kg/m^3 and the airspeed is varied from 20m/s to 32.5m/s (as in Hodges et al.[7]) to study the impact of aeroelastic effects, which increase with the dynamic pressure.

Table 5 reports the trim angle of attack and the computational time of the linear (flexible) FEM, nonlinear FEM and multibody trim solutions vs. airspeed. The trend is similar for all the three methods, the nonlinear FEM and multibody results are in good agreement, the error (FEM with respect to multibody) linearly increasing with airspeed from -4.6% to -8.5%, but there is a significant difference in the linear results, which show trim angles considerably lower. The reason is twofold. First, comparing the local angle of attack along the span due to the wing elastic twist (Figure 11, airspeed 32.5m/s), it is clear that the twist predicted by a linear structural model is higher and the wing features an unrealistic amount of wash-in (i.e. nose-up twist) that leads to an overpredicted aircraft lift-curve slope and thus to lower trim angles of attack. Secondly, a linear analysis does not take into account the follower effect on the aerodynamic forces, which results in an inboard tilt of the lift all along the wingspan and in a loss of lift effectiveness because of the reduction of its vertical component. The wing deformed shape at trim, for the minimum and maximum airspeed, is depicted in Figure 12, where the wing deformation can be seen to increase with airspeed and how this causes the loss of vertical lift.

Further insights can be gained by checking the lift distribution at 32.5m/s. Figure 13(a) shows the lift distribution along the span, plotted versus the initial wing y coordinate for the linear and versus the deformed wing y coordinate for the nonlinear results, and Figure 13(b) presents the lateral, F_Y, and vertical, F_Z, components of the lift in the global reference frame. As mentioned previously, the follower force effect leads to a lateral lift component, not predicted by the linear solution. The vertical component, in the nonlinear cases, is shifted inboard, both as a result of the smaller wash-in and of the wing end shortening. The total lift though, is higher in the nonlinear results, being the sum of these two components and explaining thus the higher trim angles of attack required.

In terms of computational time, the multibody procedure shows a distinct advantage compared to the nonlinear FEM. For the latter, the computational time increases with the airspeed since the higher the dynamic pressure the greater the wing deformation and, as a consequence, the Nastran nonlinear solver requires finer load increments and more iterations in order to converge.

Table 5. Trim angle of attack and CPU time vs. airspeed, comparison of linear FEM, nonlinear FEM and multibody trim solutions.

	Linear Trim FEM		*Nonlinear Trim FEM*		*Trim MBD*	
Airspeed [m/s]	**α [deg]**	**CPU time [s]**	**α [deg]**	**CPU time [s]**	**α [deg]**	**CPU time [s]**
20.0	9.52	<1	12.11	67.64	12.70	25.22
22.0	7.41	<1	9.69	80.90	10.23	21.05
25.0	5.12	<1	7.09	99.89	7.56	20.83
28.0	3.50	<1	5.30	143.38	5.70	14.40
30.0	2.66	<1	4.40	207.45	4.76	17.91
32.5	1.80	<1	3.57	360.20	3.86	23.76

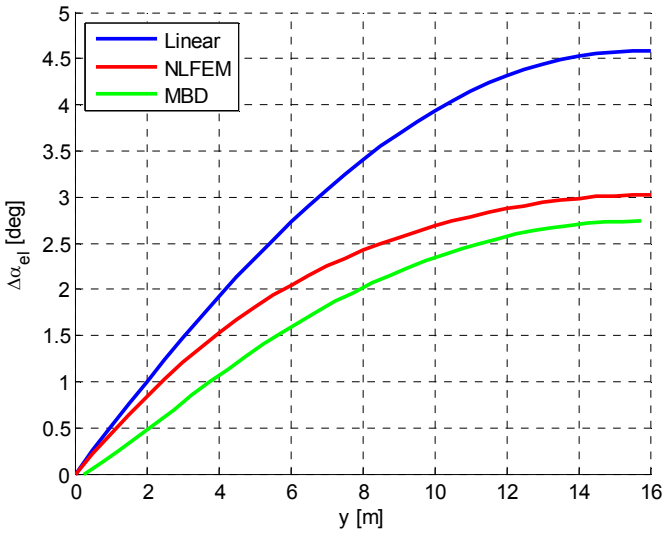

Figure 11. Wing local angle of attack due to elastic twist at 32.5m/s trim, comparison of linear and nonlinear results.

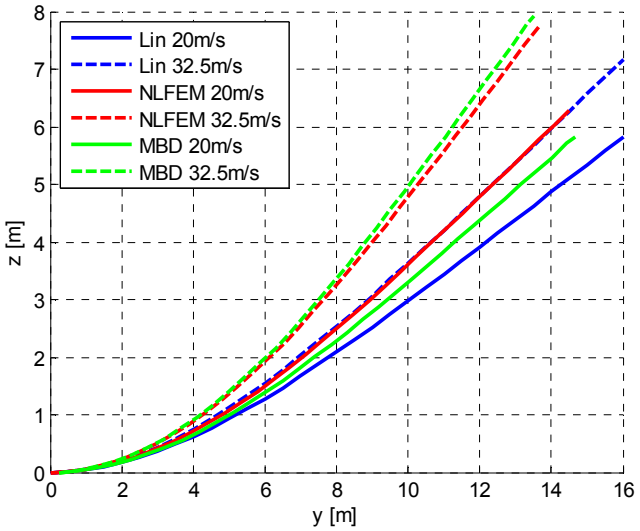

Figure 12. Wing deformed shape at 20m/s and 32.5m/s trim, comparison of linear and nonlinear results.

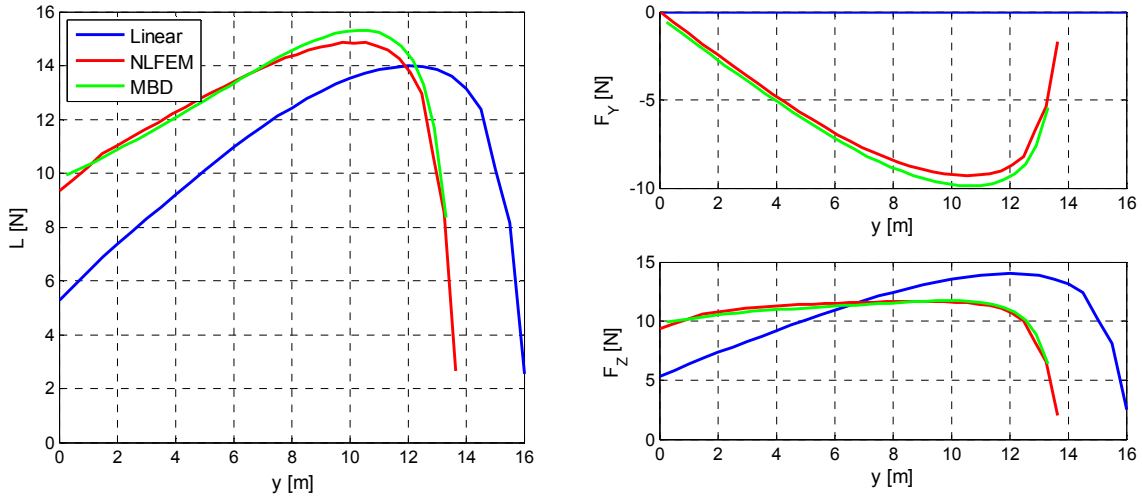

Figure 13. Lift (a) and lateral and vertical lift components (b) along the wingspan at 32.5m/s trim, linear vs. nonlinear.

The wing integrated loads are presented in Figure 14, showing the forces, and Figure 15, showing the moments. An important point to highlight for the interpretation of the results is that, in a linear approach, the integrated loads are computed based on the wing undeformed shape, whereas, in the nonlinear case, these are computed based on the actual wing deformed geometry and are expressed in the local reference frame of each beam element.

Comparing the forces, it can be noted that there is a good agreement between the nonlinear FEM and multibody on the shear distribution, the difference being within a range of +5 to -10% up to 80% span; on the other hand, the linear trim shows a lower shear.

The inboard tilt of the lift due to the follower force effect generates a significant axial load on the wing, which increases as the bending rotation increases. This is not predicted by a linear analysis and, even though the axial force itself is not critical for the wing box structure, it contributes to the bending moment.

Comparing the latter (Figure 15), both the nonlinear FEM and multibody shows a good match (difference within ±5% up to 80% span) whereas the linear analysis underpredicts it, especially at the higher speed (-14% root bending moment with respect to multibody). As previously mentioned, in the nonlinear case the bending induced by the lateral lift component acting out-of-plane overcompensates for the moment arm reduction of the vertical force following the wing end shortening.

There are nonetheless major differences between the two nonlinear methodologies in the torque, in-plane bending moment and in-plane shear prediction. In the multibody, the in-plane shear, though small in magnitude compared to the vertical shear, is non-zero. This arises from two contributions: the rotation of the lift vector, perpendicular to the airspeed, from wind to body axes and the rotation of the gravity vector from global (Earth-fixed) to body axes. The in-plane shear, and in turn in-plane bending moment, is then mainly generated following the local pitch angle rotation, sum of the aircraft trim angle of attack and twist deformation of each section.

None of these two components is taken into account by the FEM approach, which assumes, being based on DLM, an aerodynamic force always normal to the displaced aerodynamic panel and, unlike the multibody, the structural model has a constant orientation in the global FE reference frame and does not undergo rigid body motion.

It must be pointed out that the in-plane loads are generally secondary for a wing-box structure, nevertheless they may increase the stress of certain local structural elements, for instance lead to a higher compression either on the front or rear spar caps and either on the forward or aft wing-fuselage attachment links, therefore it is important to take these into account in the structural sizing.

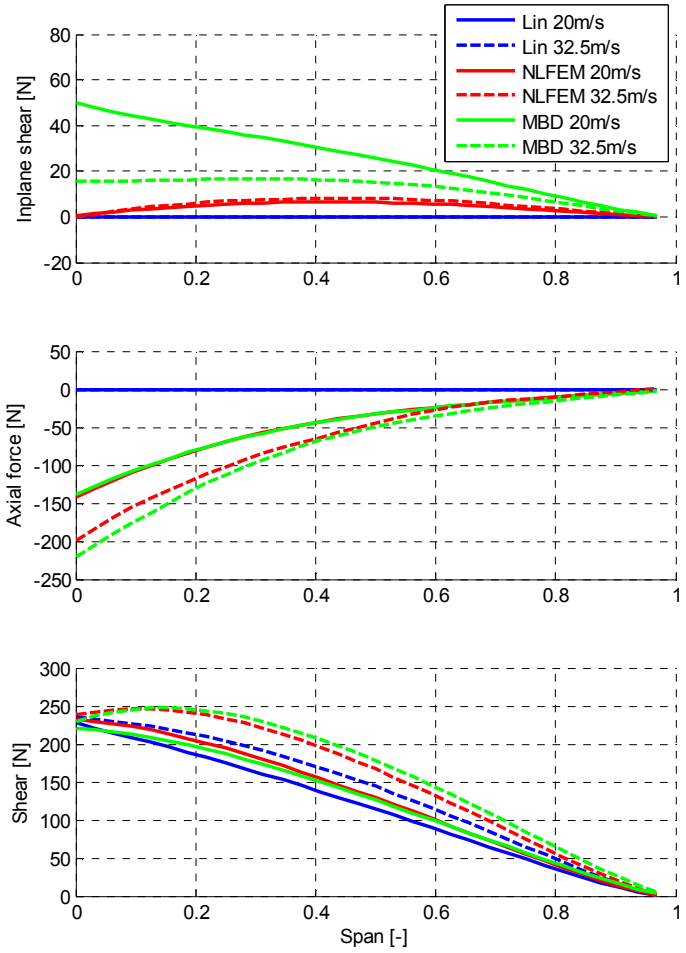

Figure 14. Wing integrated forces at 20m/s and 32.5m/s trim, comparison of linear and nonlinear results.

In order to confirm the aforementioned factors as the sources of discrepancies between the FEM and multibody trim results, the nonlinear FEM formulation is modified to include the longitudinal force due to the rotation of lift and gravity from the global to the local reference frames. By updating the rotation matrices in Eqs. (23) and (25), a longitudinal aerodynamic force in the local displaced reference frame of each structural node is applied following the pitch rotation of the node, which is due both to the elastic twist and the rigid aircraft angle of attack. Similarly, the gravity vector on the RHS of Eq. (22) is updated at each step based on the total pitch rotation of each node at the current converged configuration.

Comparing the in-plane shear, torque and in-plane bending moment from Figure 14 and Figure 15 with the modified procedure in Figure 16, it can be seen that the nonlinear FEM prediction is now closer to the multibody one thanks to the added effects.

Following the results presented, the main sources of discrepancies between a linear and nonlinear approach are identified as:

1. Large displacements and rotations: very flexible wings undergo large displacements and rotations that cannot be neglected and second order effects, such as the wing end shortening become important and have an impact on both the trim angle of attack and the flight loads. The twist is influenced as well by taking into account geometric nonlinearities and reduced compared to the linear analysis.

2. Follower force effect: aerodynamic forces, arising from pressure distributions, are inherently follower forces. The inboard tilt of the lift along the span due to the wing bending generates a lateral force component that contributes to the wing integrated loads, introducing an axial load and increasing the bending moment by compensating for the moment arm shortening of the lift vertical component, and that leads to a loss of vertical lift effectiveness. This in turn results in a higher trim angle of attack required, potentially approaching more rapidly the stall angle than in the linear case
3. Computation of wing integrated loads based on the deformed shape: the actual deformed shape is considered to compute the integrated loads along the wing, which are expressed in the local reference frame of each displaced wing section. As a consequence, for stress calculations and sizing in a typical industrial aircraft design process, it is then necessary to provide both the external loads and the wing deformed shape.

It must be however underlined that both the trend of the results and the quantitative differences between a linear and a nonlinear trim analysis are highly dependent on the configuration examined, specifically on the wing geometry (aspect ratio, sweep angle, dihedral angle, planform) and on the stiffness distribution. For these reasons, no absolute conclusion may be drawn on the impact of geometric nonlinearities on loads and this highlights the importance of performing nonlinear analyses for very flexible high aspect ratio wing aircraft.

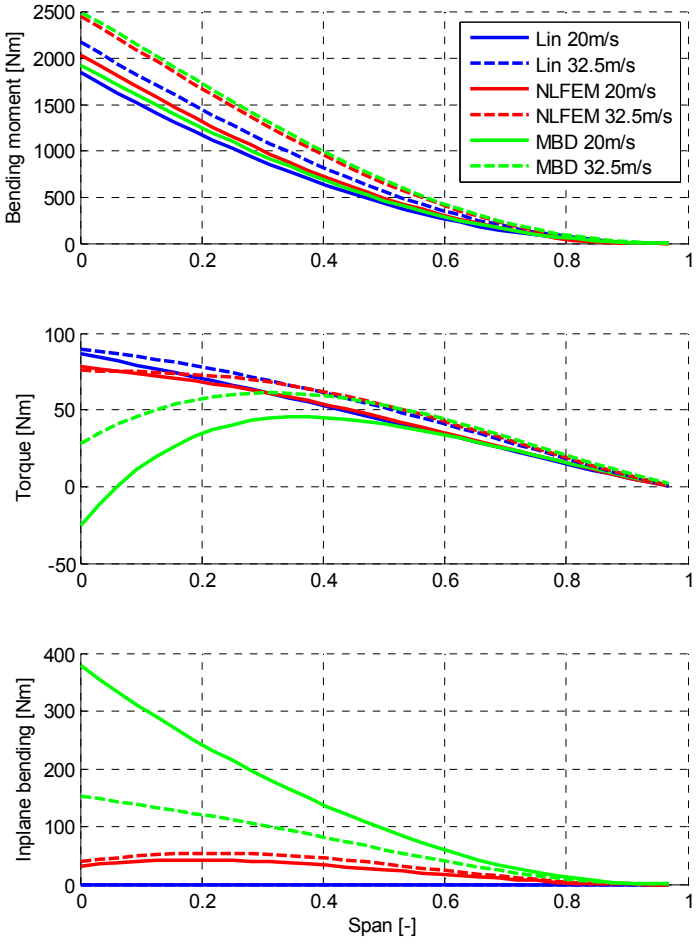

Figure 15. Wing integrated moments at 20m/s and 32.5m/s trim, comparison of linear and nonlinear results.

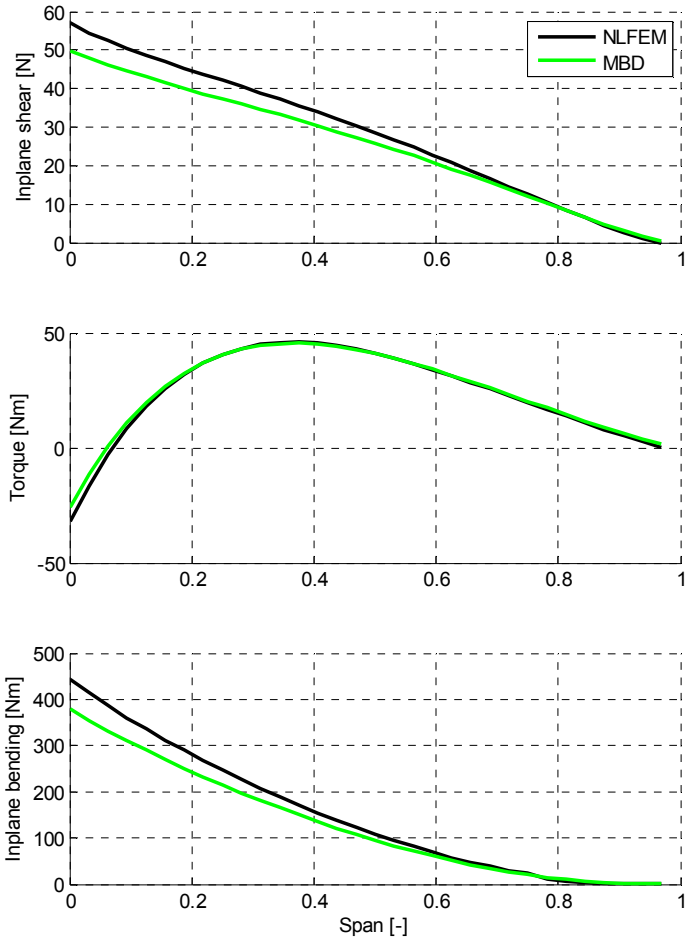

Figure 16. Wing in-plane shear, torque and in-plane bending moment at 20m/s trim, multibody vs. improved nonlinear FEM

V. Conclusion

In this paper two modelling methodologies for the nonlinear static aeroelasticity of high aspect ratio wing aircraft subject to structural nonlinearities have been presented. The first is based on the nonlinear Finite Element Method and the second on multibody dynamics. Both formulations have been extended to include steady aerodynamic forces due to the aircraft states and deformation and trim procedures have been developed. A simple test case representative of a very flexible high aspect ratio wing aircraft has been taken from the literature to compare linear vs. nonlinear results and the two nonlinear formulations.

The two methodologies are based on computational tools and software which are the current standard in the aerospace industry and not on formulations and codes developed ad-hoc for high aspect ratio wings. This should consequently facilitate the transition from linear to structural nonlinear aeroelastic analyses.

The static flight loads at various trim conditions have been compared for the linear and the two nonlinear methods and the importance of adopting a nonlinear approach demonstrated by the significant differences in the wing integrated loads.

The FEM and multibody methods show an excellent agreement for purely structural problems (static and pre-stressed normal modes). There are instead more differences in the aeroelastic trim results. The root causes of these differences have been identified in the different assumption for the aerodynamic force orientation and in the treatment of rigid body rotations. Specifically, the multibody simulation is capable of taking into account nonlinear

kinematic effects due to the large rigid body motion of the aircraft. The FEM procedure has been improved to model these missing effects and a good match on the wing integrated loads achieved.

The multibody has also demonstrated a distinct advantage in terms of computational time for the nonlinear trim analyses. It is envisaged that this could grow even further for nonlinear aeroelastic dynamic response (gust or maneuvre).

Acknowledgments

This work is supported by the European Commission (EC FP7) under the Marie Curie European Industrial Doctorate Training Network ALPES (Aircraft Loads Prediction using Enhanced Simulation – Grant Agreement No. 607911) and the Royal Academy of Engineering.

References

[1] Advisory Council for Aviation Research and Innovation in Europe, "ACARE Flighpath 2050 – Europe's Vision for Aviation," URL: http://www.acare4europe.com/documents/latest-acare-documents/acare-flightpath-2050.

[2] "The Airbus Concept Plane," URL: www.airbus.com/innovation/future-by-airbus/the-concept-plane/the-airbus-concept-plane.

[3] Bradley, M. K., and Droney, C. K., "Subsonic Ultra Green Aircraft Research," NASA/CR-2011-216847, 2011.

[4] Stodieck, O., Cooper, J. E., and Weaver, P. M., "On the Interpretation of Bending-Torsion Coupling for Swept, Non-Homogenous Wings," *Proceedings of the 56th AIAA/ASCE/AHS/ASC Structures, Structural Dynamics, and Materials Conference*, Orlando, FL, USA, January 2015.

[5] Cesnik, C. E. S., Palacios, R., and Reichenbach, E. Y., "Reexamined Structural Design Procedures for Very Flexible Aircraft," *Journal of Aircraft*, Vol. 51, No. 5, 2014, pp. 1528-1591.

[6] Livne, E., and Weisshaar, T. A., "Aeroelasticity of Nonconventional Airplane Configurations – Past and Future," *Journal of Aircraft*, Vol. 40, No. 6, 2003, pp. 1047-1065.

[7] Cesnik, C. E. S., Patil, M. J., and Hodges, D. H., "Nonlinear Aeroelasticity and Flight Dynamics of High-Altitude Long-Endurance Aircraft," *Journal of Aircraft*, Vol. 38, No. 1, 2001, pp. 88-94.

[8] Tang, D., and Dowell, E. H., "Experimental and Theoretical Study on Aeroelastic Response of High-Aspect-Ratio Wings," *AIAA Journal*, Vol. 39, No. 8, 2001, pp. 1430-1441.

[9] Garcia, J. A., "Numerical Investigation of Nonlinear Aeroelastic Efffects on Flexible High-Aspect-Ratio Wings," *Journal of Aircraft*, Vol. 42, No. 4, 2005, pp. 1025-1036.

[10] Patil, M. J., and Hodges, D. H., "Flight Dynamics of Highly Flexible Flying Wings," *Journal of Aircraft*, Vol. 43, No. 6, 2006, pp. 1790-1799.

[11] Palacios, R., Murua, J., and Cook, R., "Structural and Aerodynamic Models in the Nonlinear Flight Dynamics of Very Flexible Aircraft," *AIAA Journal*, Vol. 48, No. 11, 2010, pp. 2559-2648.

[12] Hesse, H., and Palacios, R., "Consistent Structural Linearisation in Flexible-Body Dynamics with Large Rigid-Body Motion," *Computers & Structures*, Vol. 110-111, 2012, pp. 1-14.

[13] Arena, A., Lacarbonara, W., and Marzocca, P., "Nonlinear Aeroelastic Formulation and Postflutter Analysis of Flexible High-Aspect-Ratio Wings," *Journal of Aircraft*, Vol. 50, No. 6, 2013, pp. 1748-1764.

[14] Krüger, W. R., "Multibody Dynamics for the Coupling of Aeroelasticity and Flight Mechanics of Highly Flexible Structures," *Proceedings of the IFASD*, Stockholm, Sweden, June 2007.

[15] Zhao, Z., and Ren, G., "Multibody Dynamic Approach of Flight Dynamics and Nonlinear Aeroelasticity of Flexible Aircraft," *AIAA Journal*, Vol. 49, No. 1, 2011, pp. 41-54.

[16] Lomax, T. D., *Structural Loads Analysis for Commercial Transport Aircraft: Theory and Practice*, 2nd ed., AIAA Education Series, Virginia, 1996.

[17] NX Nastran Handbook of Nonlinear Analysis, Siemens PLM Software Inc., 2013.

[18] Bathe, K.-J., *Finite Element Procedures*, 1st ed., Prentice-Hall, New Jersey, 1996.

[19] Albano, E., and Rodden, W. P., "A Doublet-Lattice Method for Calculating Lift Distributions on Oscillating Surfaces in Subsonic Flows," *AIAA Journal*, Vol. 7, No. 2, pp. 279-285.

[20] Hedman, S. G., "Vortex Lattice Method for Calculation of Quasi Steady State Loadings on Thin Elastic Wings in Subsonic Flow," *FFA Report 105*, 1966.

[21] Shabana, A., *Dynamics of Multibody Systems*, 3rd ed., Cambridge University Press, Cambridge, England, UK, 2010.

[22] Krüger, W. R., and Spieck, M., "Aeroelastics Effects in Multibody Dynamics," *Vehicle System Dynamics*, Vol. 41, No. 5, 2004, pp. 383-399.

[23] Cavagna, L., Masarati, P., and Quaranta, G., "Coupled Multibody/Computational Fluid Dynamics Simulation of Maneuvering Flexible Aircraft," *Journal of Aircraft*, Vol. 48, No. 1, 2011, pp. 92-106.

[24] LMS Virtual.Lab 13 Online Help, Rev 13, June 2014

[25] Bauchau, O. A., *Flexible Multibody Dynamics*, 1st ed., Springer, Dordrecht, Heidelberg, London, New York, 2010.

[26] Ghiringhelli, G. L., Masarati, P., and Mantegazza, P., "A Multi-Body Implementation of Finite Volume Beams," *AIAA Journal*, Vol. 38, No. 1, 2000, pp. 131-138.

[27] Bauchau, O. A., Bottasso, C. L., and Nikishkov, Y. G., "Modeling rotorcraft Dynamics with Finite Element Multibody Procedures," *Mathematical and Computer Modelling*, Vol. 33, 2001, pp. 1113-1137.

[28] Connelly, J. D., and Huston, R. L., "The Dynamics of Flexible Multibody Systems-A Finite Segment Approach. I: Theoretical Aspects," *Computer & Structures*, Vol. 50, No. 2, 1994, pp. 255-258.

[29] Demasi, L., and Livne, E., "Aeroelastic Coupling of Geometrically Nonlinear Structures and Linear Unsteady Aerodynamics: Two Formulations," *Proceedings of the 49th AIAA/ASME/ASCE/AHS/ASC Structures, Structural Dynamics, and Materials Conference*, Schaumburg, IL, USA, April 2008.

[30] Demasi, L., and Livne, E., "Dynamic Aeroelasticity of Structurally Nonlinear Configurations Using Linear Modally Reduced Aerodynamic Generalized Forces," *AIAA Journal*, Vol. 47, No. 1, 2009, pp. 71-90.

[31] Mian, H. H., Wang, G., and Ye, Z.-Y., "Numerical investigation of structural geometric nonlinearity effect in high-aspect-ratio wing using CFD/CSD coupled approach," *Journal of Fluids and Structures*, Vol. 49, 2014, pp. 186-201.

[32] Ferguson, S. D., Viisoreanu, A., Schwimley, S., and Miller, G. D., "Integrated Nonlinear Aerodynamic-Structural Tool for External Loads Development," *Proceedings of the AIAA Atmospheric Flight Mechanics Conference and Exhibit*, Hilton Head, SC, USA, August 2009.

[33] Kier, T. M., Verveld, M. J., and Burkett, C. W., "Integrated Flexible Dynamic Loads Models Based on Aerodynamic Influence Coefficients of a 3D Panel Method", *Proceedings of the IFASD 2015*, St. Petersburg, Russia, June 2015.

[34] Robinson, M., *Programming DMAP in MSC.Nastran™*, 1st ed., 2012.

[35] Prescott, W., "Steady-State Aircraft Landing Loads Analysis," *Proceedings of the 2009 ECCOMAS Thematic Conference on Multibody Dynamics*, Warsaw, Poland, June 2009.

[36] Oliver, M., Climent, H., and Rosich, F., "Non Linear Effects of Applied Loads and Large Deformations on Aircraft Normal Modes," *Proceedings of the Specialists' Meeting of the RTO Applied Vehicle Technology Panel (AVT)*, Ottawa, ON, Canada, October 1999.